Author Manuscript

Engineered Microenvironmental Cues from Fiber-reinforced Hydrogel Composites Drive Tenogenesis and Aligned Collagen Deposition

Robert N. Kent III[1], Maggie E. Jewett[1], Trevor P. Buck[1], Mohamed Said[1], LeeAnn A. Hold[3], Eileen A. Crawford, MD[3], Megan L. Killian, PhD[3], Adam C. Abraham, PhD[3], Alice H. Huang, PhD[4], Brendon M. Baker, PhD[1,2]

[1] Department of Biomedical Engineering

University of Michigan, Ann Arbor, MI 48109

[2] Department of Chemical Engineering

University of Michigan, Ann Arbor, MI 48109

[3] Department of Orthopedic Surgery

University of Michigan, Ann Arbor, MI 48109

[4] Department of Orthopedic Surgery

Columbia University, New York, NY 10027

[+] Corresponding Author:

Brendon M. Baker, Ph.D.

Department of Biomedical Engineering, University of Michigan

2174 Lurie BME Building, 1101 Beal Avenue

Ann Arbor, MI 48109

This is the author manuscript accepted for publication and has undergone full peer review but has not been through the copyediting, typesetting, pagination and proofreading process, which may lead to differences between this version and the Version of Record. Please cite this article as doi: 10.1002/adhm.202400529.

This article is protected by copyright. All rights reserved.

Email: bambren@umich.edu

Author Manuscript

Key words: tendon; tenogenesis; tendon progenitor cell; electrospinning; fiber-reinforced hydrogel composite

ABSTRACT

Effective tendon regeneration following injury is contingent on appropriate differentiation of recruited cells and deposition of mature, aligned, collagenous extracellular matrix that can withstand the extreme mechanical demands placed on the tissue. As such, myriad biomaterial approaches have been explored to provide biochemical and physical cues that encourage tenogenesis and template aligned matrix deposition in lieu of dysfunctional scar tissue formation. Fiber-reinforced hydrogels present an ideal biomaterial system toward this end given their transdermal injectability, tunable stiffness over a range amenable to tenogenic differentiation of progenitors, and capacity for modular inclusion of biochemical cues. Here, tunable and modular, fiber-reinforced, synthetic hydrogels are employed to elucidate salient microenvironmental determinants of tenogenesis and aligned collagen deposition by tendon progenitor cells. Transforming growth factor β3 drives a cell fate switch toward pro-regenerative or pro-fibrotic phenotypes, which can be biased toward the former by culture in softer microenvironments or inhibition of the RhoA/ROCK activity. Furthermore, studies demonstrate that topographical anisotropy in fiber-reinforced hydrogels critically mediates the alignment of *de novo* collagen fibrils, reflecting native tendon architecture. These findings inform the design of cell-free, injectable, synthetic hydrogels for tendon tissue regeneration and, likely, that of a range of load-bearing connective tissues.

1. *INTRODUCTION*

Tendon and ligament injuries comprise ~45% of the 124 million cases of musculoskeletal injury reported annually in the United States.[1] Particularly in adults, Achilles tendons are unable to fully regenerate following injury, resulting in comparably

This article is protected by copyright. All rights reserved.

poor outcomes regardless of surgical or conservative management.[2] Poor clinical outcomes following tendon rupture are largely attributed to the generation of disorganized, hypercellular scar tissue that causes chronic pain, fails to meet the mechanical demands of the tendon, and heightens the risk of reinjury.[3] Better approaches for treating tendon injuries are therefore desperately needed, which could be informed by contexts where regenerative tendon healing occurs naturally.

Robust tendon healing requires the recruitment, organization, and differentiation of appropriate cell types. Models of Achilles tendon injury in neonatal C57BL/6 and adult MRL/MpJ mice demonstrate recruitment of tendon progenitor cells (TPCs), which undergo tenogenic differentiation and regenerate functional tissue.[4] Although tendon progenitor cells exist in the adult C57BL/6 mouse and human epitenon[4a, 5], they contribute to both tenogenic and fibrogenic cell populations; the latter is thought to drive formation of disorganized, dysfunctional scar tissue, which is mechanically inferior and prone to reinjury.[3a, 4a, 5a] New therapies that can drive tenogenic (and prevent fibrogenic) differentiation of recruited progenitors and provide a template for aligned matrix deposition could therefore result in improved functional regeneration of tendon and greatly reduce the economic burden of these injuries.

Toward this end, prior strategies have focused on the delivery of tenogenic drugs and biologics via injection or suture-based delivery.[6] While demonstrating promising biological responses, these approaches failed to template organized collagen deposition within the healing tissue.[7] Aligned, fibrous scaffolds can provide such a template and even approach the mechanical properties of native tendon upon implantation, but they exhibit poor tissue integration and drive aberrant cell differentiation, adversely impacting tissue regeneration.[8] Synthetic hydrogels therefore represent an exciting avenue in the field of regenerative biomaterials given their transdermal injectability, tunable mechanical properties, and potential for modular inclusion of physical and soluble microenvironmental cues to drive regenerative biology.[9] Moreover, fiber-reinforced hydrogel composites (FRHCs) allow for orthogonal tuning of bulk mechanical properties and fibrous topography, simultaneously providing (1) a soft microenvironment amenable to tenogenesis and inhibitory to myofibroblastic differentiation, and (2) organized fibrous topography to template *de novo* matrix deposition.[10] Previous work from our lab has shown that fiber-

This article is protected by copyright. All rights reserved.

Author Manuscript

reinforced, synthetic hydrogels are amenable to the recruitment of TPCs from the epitenon of adult murine Achilles tendons.[11] This injectable composite demonstrated synergistic, pro-migratory effects of fibrous topography and microgel-delivered platelet-derived growth factor BB on TPCs, with a majority of recruited cells expressing *Scleraxis* (*Scx*), an early and critical tenogenic transcription factor.[4b, 4c, 12]

Building on this work, here we systematically developed 2D then 3D engineered culture platforms to identify salient topographical, adhesive, and soluble cues that drive tenogenic differentiation of TPCs in addition to aligned, collagenous matrix production reflecting the matrix architecture of native tendon. To delineate biological processes central to tendon regeneration in 3D, we designed cell-degradable FRHCs imbued with topographical cues by incorporating cell-adhesive fiber segments.[10a, 11] We confirmed observations from previous studies that TGF-β is tenogenic,[4b, 4e, 4f, 13] but also elucidated microenvironmental determinants of a fate switch between myofibroblastic vs. tenogenic differentiation. Finally, we applied FRHC design features optimized with murine TPCs and found that human tendon-derived cell (TDC) tenogenesis and matrix production appears to be highly contingent on the extent and chronicity of tendinopathy in the tissue from which cells are derived. Collectively, these findings provide fundamental insights into the microenvironmental cues that promote tenogenesis and define key material design parameters of injectable, fibrous hydrogel composites for improved tendon regeneration.

2. *MATERIALS AND METHODS*

Reagents: All reagents were purchased from Sigma-Aldrich or Fisher Scientific and used as received, unless otherwise stated.

Cell isolation and culture: For all animal procedures, the Institutional Animal Care and Use Committee (IACUC) guidelines for survival surgery in rodents and the IACUC Policy on Analgesic Use in Animals Undergoing Surgery were followed (Protocol #PRO00009868). Murine cells used in this work were harvested from 12 6-9 week-old C57BL/6 mice (6

This article is protected by copyright. All rights reserved.

Author Manuscript

female, 6 male). A ScxGFP mouse colony was maintained by breeding $ScxGFP^{+/-}$ heterozygotes modified from a C57BL/6 background with WT C57BL/6J mice, and progeny were genotyped ($ScxGFP^{+/-}$ vs. $ScxGFP^{-/-}$) using a Dual Fluorescent Protein Flashlight (Model DFP-1, Nightsea, Lexington, MA). Tail tendons were removed from euthanized mice and then encapsulated in a 2 mg mL^{-1} type I collagen hydrogel. Encapsulated tissues were cultured in an incubator (37°C and 5% CO_2) in DMEM containing L-glutamine (ThermoFisher, Waltham, MA), 1 v/v% penicillin/streptomycin/fungizone, and 10 v/v% fetal bovine serum (termed 'basal media') for 10 days to allow tendon progenitor cells (TPCs) to migrate from tendons into the collagen gel.[14] Following isolation and expansion of TPCs, collagen gels were digested in 0.25 mg mL^{-1} collagenase from *C. histolyticum* with 0.025 w/v % trypsin-EDTA. The resulting slurry was filtered through a cell strainer and then plated. Adherent TPCs were cultured in basal media, and cells at passage 1 were used for all experiments. For studies where cell proliferation was inhibited, TPC cultures were treated with 40 μg mL^{-1} mitomycin C for two hours, washed with basal media, then incubated for at least one hour prior to trypsinization for use in studies.

Human tendon-derived cells (TDCs) were isolated from multiple sources in accordance with Institutional Review Board guidelines. One cell population was isolated from a chronically tendinopathic, proximal bicipital tendon that was harvested by a board-certified sports medicine surgeon (E.A.C.) during a biceps tenodesis (Protocol #HUM00226997). Two other populations were isolated from Achilles tendon tissue acquired during insertional debridement and repair procedures by a board-certified foot and ankle surgeon (P.G.T.) (Protocol #HUM00196928). All human TDCs were isolated from their respective tissues using previously described methods.[14-15]

Polymer synthesis: Dextran functionalized with vinyl sulfone groups (DexVS) was synthesized as previously described.[16] Briefly, 5 g of 86 kDa dextran (MP Biomedicals, Irvine, CA) was dissolved in a 250 mL solution of 100 mM sodium hydroxide in Milli-Q water. On a stir plate set to 700 rpm, divinyl sulfone (Alfa Aesar, Haverhill, MA) was added to the solution, and the reaction proceeded for 3.5 minutes before termination by addition of 2.5 mL of 12 M hydrochloric acid. To achieve vinyl sulfone / dextran repeat unit ratios appropriate for

This article is protected by copyright. All rights reserved.

Author Manuscript

hydrogel formation (16%) and fiber fabrication (65%), 3.88 mL and 12.5 mL of divinyl sulfone were added to the reactions, respectively. After vinyl sulfone addition, the product was dialyzed against Milli-Q water for 72 hours with twice-daily changes and then lyophilized for 72 hours to yield a dry product. All reaction products were characterized via ^{1}H NMR.

2D cell culture: For initial 2D studies screening tenogenic growth factors, glass coverslips were UV/ozone treated for 5 minutes prior to being incubated at 37°C in phosphate-buffered saline (PBS) containing 50 μg mL^{-1} fibronectin (Corning, Corning, NY) for 15 minutes. Fibronectin-functionalized coverslips were washed twice with PBS and then seeded with a suspension of TPCs in basal media (13,500 cells cm^{-2}).

To generate fiber-coated coverslips, an electrospinning solution was prepared containing 0.7 g mL^{-1} DexVS (65% vinyl sulfone functionalization) in 1:1 dimethyl formamide and Milli-Q water with 0.6 wt/v% lithium phenyl-2,4,6-trimethylbenzoylphosphinate (LAP; Colorado Photopolymer Solutions, Boulder, CO) photoinitiator, and (1) 2.5 v/v% methacrylated rhodamine (25 mM; Polysciences, Inc., Warrington, PA) for fluorescent visualization or (2) 5.0 v/v% glycidyl methacrylate when fluorescent labeling was not required. In a humidity-controlled glovebox (21°C, 30-35% humidity), DexVS fibers (1 μm diameter)[17] were electrospun onto 18 mm glass coverslips mounted to a grounded mandrel with a gap distance of 7 cm, voltage of -5.5 kV, and a flow rate of 0.2 mL hr^{-1}. The mandrel was rotated at 100 rpm (0.92 m s^{-1} surface speed) or 2100 rpm (19.3 m s^{-1} surface speed) to respectively yield random and aligned fiber orientations. Fibers were primarily photocrosslinked dry (100 mW cm^{-2} UV light) for 2 minutes and then secondarily crosslinked in a solution of 1 mg mL^{-1} LAP for 20 seconds. Coverslips were then washed twice with PBS and then incubated at 37°C for 15 minutes in a 1.0 mM solution of cell-adhesive CGRGDS (RGD) in 50 mM 4-(2-hydroxyethyl)-1-piperazineethanesulfonic acid (HEPES) buffer containing 10 μg mL^{-1} phenol red and buffered to a pH of 8.0 with sodium hydroxide. RGD-functionalized fiber-coated coverslips were then washed twice with PBS prior to seeding with a suspension of TPCs in basal media (13,500 cells cm^{-2}).

Author Manuscript

This article is protected by copyright. All rights reserved.

Fiber segment fabrication and functionalization for FHRCs: An electrospinning solution was prepared by dissolving DexVS (65% vinyl sulfone functionalization) at 0.7 g mL^{-1} in a 1:1 solution of dimethyl formamide and Milli-Q water with 0.015 wt/v% 2-Hydroxy-4'-(2-hydroxyethoxy)-2-methylpropiophenone (Irgacure 2959) photoinitiator. For fluorescent visualization of fibers, methacrylated rhodamine (Polysciences, Inc., Warrington, PA) was added at 0.5 mM. In the same humidity-controlled glovebox described above, DexVS fibers were electrospun onto a slowly rotating (linear velocity 3.14 cm s^{-1}), grounded mandrel using a gap distance of 7 cm, voltage of -5.5 kV, and flow rate of 0.2 mL hr^{-1}. A UV lamp was directed at the opposite side of the mandrel; every 15 minutes, the lamp was turned on for 5 minutes to expose deposited fibers to 100 mW cm^{-2} UV light. Intermittent UV exposure over the course of layer-by-layer fiber deposition ensured that fibers were adequately and uniformly photocrosslinked. The resulting fiber segments had the same diameter as those spun onto glass coverslips for 2D studies (1 μm diameter).[17]

The crosslinked fiber mat was removed from the mandrel and transferred to Milli-Q water. Two rounds of pipetting, vortexing, centrifugation, and resuspension were performed to break up the fiber mat into individual fiber segments and remove clumps and residual crosslinking reagents. Purified fibers were resuspended at 10 v/v% in PBS and stored in a light-protected box at 4°C. Prior to incorporation in hydrogel constructs, fiber segments were functionalized by resuspension at 10 v/v% in 50 mM HEPES buffer along with cell-adhesive CGRGDS (RGD) (2.0 mM) and 5 mM sodium hydroxide. Functionalization proceeded via Michael-type addition at 37°C for 15 minutes, then fibers were washed with PBS and resuspended in HEPES buffer.

Fabrication of FRHCs: DexVS hydrogels were formed using previously described methods.[10a] Briefly, DexVS was dissolved in PBS containing 50 mM HEPES buffer. Either cell-adhesive RGD or scrambled CGRDGS (RDG) was incorporated at 2.0 mM. Additionally, to neutralize residual VS groups and prevent unintended crosslinking, cysteine was added at 9.1 mM. After this pre-reaction proceeded on ice for 20 minutes, cells and functionalized fiber segments were added to the mixture followed by the addition of an MMP-cleavable, dithiolated GCRDVPMSMRGGDRCG (VPMS) crosslinking peptide. Bulk stiffnesses ranging

This article is protected by copyright. All rights reserved.

Author Manuscript

from 0.5-6 kPa were achieved by crosslinking DexVS hydrogels with 12.5-27.5 mM VPMS, respectively; DexVS concentrations of 3.30-4.13 wt/v% were used to ensure that the ratio of free vinyl sulfone groups to VPMS molecules were consistent across crosslinking densities.[17] Gelation via Michael-type addition was initiated by addition of sodium hydroxide (33 mM).

Hydrogel composites were cast in circular molds to generate gels with isotropic fibrous topography. Polydimethylsiloxane (PDMS) (Dow, Midland, MI) was prepared at a 1:10 crosslinker:base ratio, casted, and biopsy-punched to form circular molds (5 mm diameter, 1.8mm height). Molds were plasma etched, bonded to 18 mm glass coverslips, coated with a solution of 2 mg mL^{-1} porcine skin gelatin (to enable eventual de-adhesion from the hydrogel), and dried in an 80°C oven for 20 minutes. 35 µL of FHRC precursor suspension was added to each mold, and crosslinking proceeded at 37°C for 45 minutes. A rotisserie rotated the sample at 5 rpm to prevent cells and fibers from settling under gravity prior to gelation. After crosslinking, FHRCs were hydrated in basal media and released from the molds the following morning.

A 4-channel microfluidic chip was designed to flow-align fibers within FHRCs. The device was designed in SolidWorks (Dassault Systèmes, Vélizy-Villacoublay, France), and a master mold was 3D printed via a Formlabs Form 3 stereolithography printer with v4 resin (Formlabs, Somerville, MA). Printed molds were treated with trichloro(1H,1H,2H,2H-perfluorooctyl)silane to facilitate release of PDMS replica casts (1:25 crosslinker:base ratio). The softer PDMS was used in this instance to allow for an airtight seal to be formed with a glass coverslip without the need for plasma etching so that the molds could be easily removed after hydrogel crosslinking. 3 mm and 1.5 mm holes were punched in the inlet and vacuum ports of the device (**Figure 5**C), respectively, then devices were washed with isopropanol followed by ethanol. The device's 500x500 µm channels were coated with 2 mg mL^{-1} porcine skin gelatin and dried in an 80°C oven for 20 minutes to facilitate eventual de-molding of the FHRC. An 18 mm glass coverslip was plasma etched for 2 minutes and then functionalized with 3-mercaptopropyl triethoxysilane via overnight gas deposition so that the FHRC could covalently adhere to the coverslip via Michael-type addition. Molds were adhered noncovalently to thiolated coverslips, 30 µL hydrogel mixtures were added to the

This article is protected by copyright. All rights reserved.

Author Manuscript

inlet ports, and gels were flowed into the devices using a syringe pump withdrawing 250 µL s^{-1}. Some gel was allowed to remain in the loading port so that there was a matched, isotropic region of the hydrogel to compare to the anisotropic regions within channels (**Figure 5**C). Crosslinking then proceeded in a 37°C rotisserie oven for 20 minutes, then devices were transferred to a 12-well plate in 1 mL of basal media and incubated at 37°C for an additional 25 minutes. Finally, PDMS molds were peeled from the coverslips, leaving the crosslinked FHRC (containing isotropic and anisotropic regions) covalently adhered to the glass.

Real-time quantitative PCR: Total RNA was isolated using Trizol reagent followed by phenol-chloroform separation. RNA yield was quantified using a Nanodrop spectrometer (ND-1000, Nanodrop Technologies, Wilmington, DE) in addition to A260/A280 to confirm a value between 1.6 and 2.1 for each isolate. cDNA was synthesized at 40-50 ng μL^{-1} using the SuperScript First Strand Synthesis kit (Invitrogen, Life Technologies, Carlsbad, CA), and cDNA samples were diluted to 0.2-0.8 ng μL^{-1} in amplification reactions solutions. Amplification was carried out using an Eppendorf Nexus GX2 thermocycler (Eppendorf, Hamburg, DE), with intron-spanning primers and Fast SYBR Green Reaction Mix (Applied Biosystems, Foster City, CA). Expression of genes of interest were determined and normalized to the housekeeping genes 40S ribosomal protein S29 (*S29*) or glyceraldehyde-3-phosphate dehydrogenase (GAPDH) for mouse and human samples, respectively, using the comparative Ct method.

For 3D cultures in DexVS hydrogel composites, single-cell suspensions were isolated prior to lysis in Trizol. A digestion solution was prepared in Accutase (Gibco, Billings, MT) containing 3 v/v% dextranase (Cellendes, Kusterdingen, Germany), 2 v/v% liberase, 0.5 mg mL^{-1} collagenase from *C. histolyticum*, and 2 mM ethylene glycol-bis(β-aminoethyl ether)-N,N,N',N'-tetraacetic acid. Hydrogel composites were washed at 37°C in DMEM for 30 minutes to remove serum proteins and then transferred to the digestion solution (1 mL of digestion solution for every 105 µL of hydrogel). Digestion proceeded in a bacteria shaker set to 37°C and 300 rpm for 20-25 minutes. Digests were diluted in 5 mL of basal media,

This article is protected by copyright. All rights reserved.

Author Manuscript

strained through a 70 µm filter, centrifuged at 500 g for 4 minutes, and resuspended in Trizol. RT-qPCR analysis was then performed as above.

Orthohydroxyproline assay: Hydrogel composites were flash-frozen at -80°C, lyophilized, then weighed to determine dry weights. Samples were then digested in papain[18], and collagen content was determined via an orthohydroxyproline assay using previously described methods.[19] Briefly, papain digests were hydrolyzed in 6N HCl at 110°C in sealed ampoules for 16 hours. The hydrolyzed product was then dried in a vacuum over NaOH for 8 hours and then resuspended in a buffer containing citric acid monohydrate (5 wt/v%), acetic acid (1.2 v/v%), and sodium acetate trihydrate (12 wt/v%). 150 µL of samples and standards, serially diluted in buffer, were added to a 96-well plate, 75 µL of chloramine T solution was added to each well, then the plate was incubated at room temperature for 20 minutes. 75 µL of p-dimethylaminobenzaldehyde solution was then added, the plate was incubated in a 70°C water bath for 20 minutes, then the plate was cooled in an ice bath prior to reading absorbance at 540 nm. Hydroxyproline content was converted to collagen using a factor of 7.14.[20] This conversion factor is an estimate and is therefore susceptible to slight bias based on the prevailing collagen type present.

Histology: Paraformaldehyde-fixed composite hydrogels were incubated in 30 wt/v% sucrose in PBS at 4°C overnight and then embedded in optimal cutting temperature (OCT) compound (SCIgen, Sunnyvale, CA) containing 30 wt/v% sucrose. After freezing on a bed of crushed dry ice, glass coverslips were removed from the embedded construct. Samples were then embedded in a larger block of OCT and then sectioned at 12 µm thickness (CM3050 Cryotome, Leica Microsystems, Wetzlar, Germany). Picrosirius Red staining was performed on sectioned samples to visualize fibrillar collagen content.

Portions of the two human Achilles tendon samples were separated prior to TDC isolation for tendinopathy scoring. These sample portions were fixed in 4% paraformaldehyde at 4°C, and paraffin-embedded sections (6 µm thickness) were stained with Hematoxylin and Eosin. Bonar scores were calculated based on cell morphology,

This article is protected by copyright. All rights reserved.

Author Manuscript

collagen arrangement, cellularity, vascularity, and the presence of ground substance.[21] QuPath software was used to quantify cellularity and evaluate for presence of ground substance.[22]

Microscopy and image analysis: Fluorescent images were captured on a Zeiss LSM800 confocal microscope. Samples were fixed in 4% paraformaldehyde, permeabilized in Triton X, and stained with phalloidin (Invitrogen, Waltham, MA) and Hoechst 33342 to visualize F-actin and nuclei, respectively. For studies assessing the extent of myofibroblastic differentiation, samples were stained with an antibody against α-smooth muscle actin (αSMA [1A4] mouse anti-mouse, ab7817, Abcam, Cambridge, UK). For studies examining focal adhesions, samples were simultaneously fixed and permeabilized at 37°C for 10 minutes; samples were then stained with an antibody against vinculin (vinculin [hVIN-1], mouse anti-mouse, V9264, Sigma Aldrich, St. Louis, MO). All FOVs acquired were mutually exclusive. To quantify fluorescent intensity in TPC monolayers, custom MATLAB code (MathWorks, Portola Valley, CA) was developed to quantify intensity within nuclei and in the cytosolic region immediately surrounding each nucleus. To quantify fluorescent intensity in 3D, Gaussian filters were applied to all images to remove noise and background. A custom MATLAB code demarcated nuclear and cytosolic regions (via Hoechst and F-actin stains) and quantified fluorescent intensity in voxels comprising each nucleus and cytosol. In general, nuclear ScxGFP was brighter than cytosolic ScxGFP, potentially implying an intact nuclear localization sequence in the transgene construct that allows for active nuclear transport of ScxGFP (**Figure 6**A; Figure S5, Supplemental Information).

Brightfield (10x) and polarized light (40x) images of Picrosirius Red-stained hydrogel sections were acquired on a Zeiss Axioplan 2 upright microscope. A rotating stage was used to acquire images from -45° to 45° of deviation at 5° intervals, where deviation denotes orientation the long axis of the flow channel relative to the polarizer in aligned regions. For non-aligned (random) regions, a deviation of 0° was defined as the orientation showing the brightest birefringence. All FOVs acquired were mutually exclusive. Custom MATLAB code identified hydrogel regions in each image and quantified red intensity as the ratio of red to the sum of red, green, and blue intensity of each pixel. Another script identified a circular

This article is protected by copyright. All rights reserved.

Author Manuscript

region of interest (100 μm radius) at the center of each polarized light image and quantified birefringent intensity as the average luminance within this region at each interval of angular deviation.

Statistics: Statistical significance was determined by one- or two-way analysis of variance (ANOVA) with Tukey's multiple comparisons test or two-sided student's t-test where appropriate ($\alpha = 0.05$). Datapoints were defined as outliers if they were >1.5 interquartile ranges from the median and excluded prior to statistical comparison. Sample size is indicated within corresponding figure legends (n technical replicates; N biological replicates), and all data are presented as mean ± standard deviation.

Data availability: The data that support the findings of this study are available from the corresponding author upon reasonable request.

3. *RESULTS AND DISCUSSION*

3.1. TGF-β2 and -β3 induce ScxGFP expression in TPCs

Murine TPCs were harvested from C57BL/6 *ScxGFP* reporter mice using previously described methods (**Figure 1**A).[14-15] This mouse, developed by Pryce et al., was created by injecting into fertilized eggs a transgene construct inserted into the first exon of *Scx*.[23] While this mouse cannot report accessibility and expression of the native *Scx* locus, it can serve as a screening tool for identifying microenvironmental cues that promote *Scx* expression and support tenogenesis. For the sake of throughput in screening potential tenogenic growth factors (GFs) at concentrations identified previously in the literature,[24] initial studies were performed with *ScxGFP* reporter TPCs cultured on fibronectin-coated glass coverslips. As evidenced by elevated *ScxGFP* expression, TGF-β most potently drove tenogenic differentiation among the GFs investigated, with TGF-β3 being the most tenogenic of the three TGF-β isoforms (**Figure 1**B-C, F). While TGF-β-induced tenogenesis

This article is protected by copyright. All rights reserved.

Author Manuscript

Author Manuscript

was further substantiated by increased expression of *Scx*, t*enascin C* (*Tnc*), and *collagen 1a2* (*Col1a2*) via qPCR, other canonical genes associated with tenogenesis including *tenomodulin* (*Tnmd*), *mohawk* (*Mkx*), *fibromodulin* (*Fmod*), *biglycan* (*Bgn*), *decorin* (*Dcn*), *collagen 1a1* (*Col1a1*), and *collagen 3a1* (*Col3a1*) were downregulated or showed no change (**Figure 1**D).[5b] Live imaging of the *ScxGFP* reporter suggested that TGF-β-induced, early tenogenesis requires ~6 days to occur (**Figure 1**E-F), and therefore all subsequent differentiation studies were performed over one week.

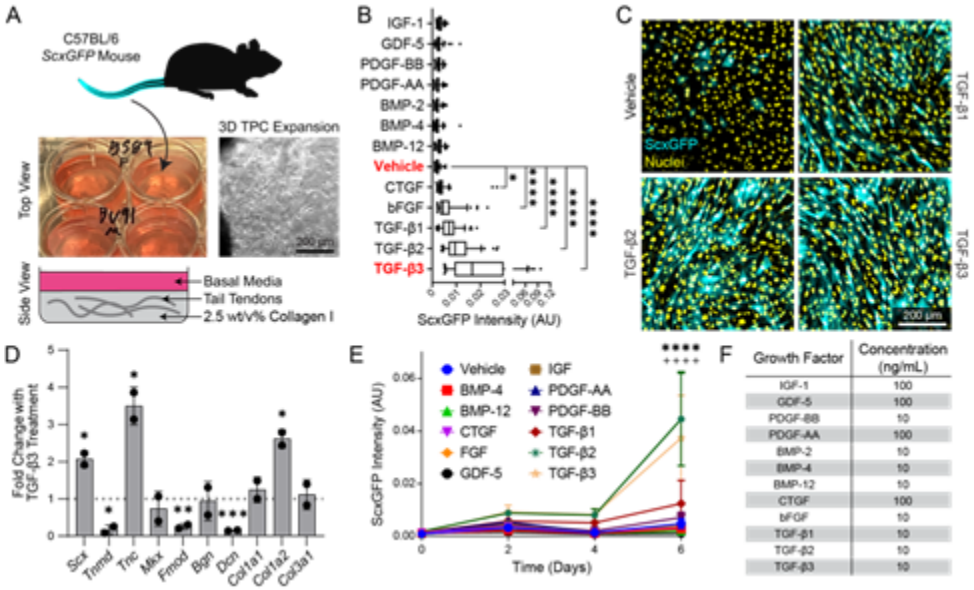


Figure 1 | TGF-β2 and -β3 induce *ScxGFP* expression in murine TPCs. A, Protocol schematic for isolating TPCs from *ScxGFP* mouse tail tendons; tendons were harvested and encapsulated in a type I collagen hydrogel, expanded in 3D for 10 days, then plated on polystyrene dishes for standard cell culture. **B,** ScxGFP intensity (AU) in TPCs cultured on fibronectin-coated glass for 7 days in media supplemented with a panel of putative tenogenic growth factors (n = 300-400 cells, N = 2). Boxes denote medians and span interquartile ranges; whiskers span 95% confidence intervals. **C,** Representative fluorescent images of TPC monolayers treated with basal media or supplemented with various TGF-β isoforms. **D,** Fold change in expression of canonical tenogenic genes with TGF-β3 treatment of TPC monolayers for 7 days (n = 2 cultures, N = 3). A fold change of 1 is denoted with a black, dotted line. **E,** Time-lapse imaging of ScxGFP intensity (AU) over the course of a 6-day TPC culture in media supplemented with a panel of growth factors (n = 6 fields of view [FOVs]). Statistical indicators represent comparisons between the vehicle control and TGF-β2 (*) or TGF- β3 (+). **F,** Table of growth factors and respective concentrations supplemented to culture media in (B-E). Unless stated otherwise, all data are reported as mean ± standard deviation. Asterisks indicate statistically significant comparisons, with *p<0.05, **p<0.01, ***p<0.001, and ****p<0.0001 by ordinary one-way ANOVA with Tukey's multiple comparisons test or Student's t-test.

3.2. Organization of fibrous topography influences tenogenic differentiation of TPCs in 2D

This article is protected by copyright. All rights reserved.

Author Manuscript

Having confirmed a soluble, biochemical driver of TPC tenogenesis, we began to interrogate the role of physical microenvironmental cues in supporting or attenuating this differentiation program. Previous work has demonstrated the potential of topographical anisotropy for promoting a tenogenic phenotype *in vitro* in TPCs and mesenchymal stem cells, which is intuitive given the highly aligned ECM of native tendon.[8e, 25] To investigate the role of topographical alignment in TGF-β3-induced tenogenesis of TPCs, we electrospun non-aligned or aligned dextran vinyl sulfone (DexVS) fibers onto glass substrates, functionalized fibers with cell-adhesive CGRDGS (RGD) peptide, then seeded and cultured TPCs with exogenous TGF-β3 (**Figure 2**A). These fibers have been shown to have similar diameter to collagen fibers *in vivo*, with both having a diameter of ~1 μm.[17] To our surprise, we found that *ScxGFP* expression did not vary as a function of topographical alignment in this context (**Figure 2**B), contrasting findings from previous work.[8e, 25] Even when seeded at a low density (13,500 cells cm^{-2}), TPCs rapidly achieved confluency on these substrates over the course of one week, likely due to the known mitogenic effects of TGF-β on mesenchymal cells[26]. Confluent TPCs achieved a spindle, uniaxial morphology with evident co-alignment to neighboring cells, independent of fiber alignment (**Figure 2**B, D; Figure S1D, Supplemental Information).[27]

To better maintain TPC morphology reflecting the topographical alignment of underlying matrix fibers, TPCs were pre-treated with mitomycin C to prevent cell proliferation over the course of the study (Figure S1A, Supplemental Information). Now-individualized TPCs demonstrated a spindle morphology on aligned substrates, coincident with increased *ScxGFP* expression compared to TPCs cultured on non-aligned fibers (**Figure 2**C, E). Fiber alignment showed minimal effects on nuclear morphology, with TPCs exhibiting similar nuclear areas and eccentricities independent of mitomycin C treatment and substrate alignment (Figure S1B-C, Supplemental Information).[28] Together, these results support prior findings that a spindle, uniaxial morphology, which can be encouraged by but does not necessarily require alignment of cell-adhesive fibers, is a critical determinant of TPC tenogenesis.

This article is protected by copyright. All rights reserved.

Author Manuscript

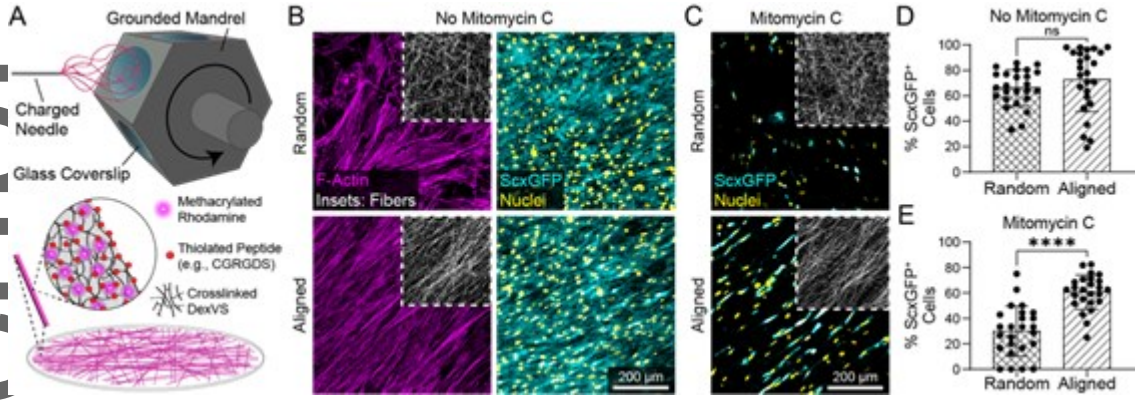


Figure 2 | Adhesive anisotropy influences TPC tenogenesis in 2D only when cell proliferation is limited. A, Schematic of DexVS fiber-coated coverslip fabrication. A solution of DexVS and methacrylated rhodamine was electrospun onto coverslips mounted to a grounded, rotating mandrel, with mandrel rotation speed dictating the resulting alignment of deposited fibers; fibers were crosslinked then functionalized with cell-adhesive CGRGDS. **B,** Fluorescent images of TPCs seeded on random or aligned substrates and cultured with TGF-β3 for one week (n = 25 FOVs, N = 3). **C,** Fluorescent images of mitomycin C pre-treated TPCs in the same culture conditions as in (B) (n = 25 FOVs, N = 2). Quantification of % of TPCs expressing *ScxGFP* (**D**) without mitomycin C pre-treatment and (**E**) with mitomycin C pre-treatment. All data are reported as mean ± standard deviation. Asterisks indicate statistically significant comparisons, with ****p<0.0001 by Student's t-test (ns denotes a non-significant comparison).

3.3. TGF-β isoforms differentially regulate tenogenic vs. myofibroblastic differentiation

Our work and others' have demonstrated the tenogenic potential of TGF-β ligands;[4b, 13] however, TGF-β signaling is known to induce myofibroblastic differentiation in a range of mesenchymal cell types, including TPCs.[29] Having observed differential promotion of *ScxGFP* expression as a function of TGF-β isoform (**Figure 1**), we next explored the capacity of TGF-β1, -β2, and -β3 to induce tenogenic vs. myofibroblastic differentiation of TPCs. Screening these isoforms again, with TPCs adhering to aligned fibers, we found that TGF-β1 uniquely promoted robust F-actin stress fiber formation (**Figure 3**A-B), suggesting heightened cytoskeletal contractility previously associated with myofibroblastic differentiation.[30] While all three isoforms resulted in increased αSMA production relative to vehicle controls, this increase was most attenuated with TGF-β3 treatment as compared to the other isoforms (**Figure 3**C, E). As in the initial screen performed on glass (which lacked topography) (**Figure 1**), all three isoforms resulted in heightened *ScxGFP* expression compared to the vehicle control (**Figure 3**D). This implied fate switch highlights the potential for TGF-β3 in promoting a regenerative phenotype following tendon injury, where tenogenic differentiation and resulting tissue regeneration may be favored over myofibroblastic

This article is protected by copyright. All rights reserved.

differentiation and disorganized scar formation.[4a] However, despite its demonstrated efficacy *in vitro,* TGF-β3 alone has been shown to drive fibrosis in lieu of functional tendon regeneration *in vivo*,[29c] and so we went on to explore additional microenvironmental cues and their interaction with TGF-β3-mediated tenogenesis vs. myofibroblastic differentiation.

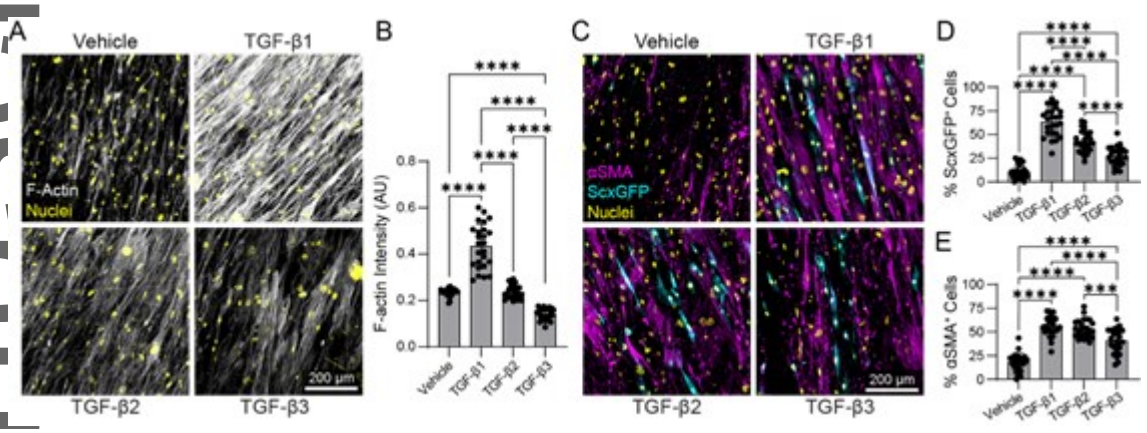


Figure 3 | TGF-β isoforms differentially regulate a tenogenic vs. myofibroblastic fate switch. TPCs were cultured for 7 days on aligned fiber-coated coverslips in basal media or supplemented with various isoforms of TGF-β. **A,** Fluorescent images of TPCs stained for F-actin . **B,** Quantification of F-actin intensity (AU) (n = 25 FOVs, N = 2). **C,** Fluorescent images of *ScxGFP* reporter TPCs stained for αSMA. Quantification of % of TPCs expressing (**D**) *ScxGFP* and (**E**) *αSMA* (n = 25 FOVs, N = 2). All data are reported as mean ± standard deviation. Asterisks indicate statistically significant comparisons, with ***p<0.001 and ****p<0.0001 by ordinary one-way ANOVA with Tukey's multiple comparisons test or Student's t-test.

3.4. TGF-β3-induced tenogenesis is a mechanosensitive process dependent on actomyosin contractility

To determine whether the contractile state of TPCs impacts tenogenic vs. myofibroblastic differentiation in response to TGF-β, we next interrogated direct regulators of actin organization and dynamics to elucidate cytoskeletal mediators of this fate switch.[31] Over the course of 7 days, TPCs on aligned fibrous substrates were supplemented every 48 hours with a small molecule agonist of Rho/Rho-kinase (ROCK) (lysophosphatidic acid [LPA]) or inhibitors of Rho/ROCK (Y27632 or H1152), Rac1 (NSC23766), Cdc42 (ML141), or myosin activity (blebbistatin) (**Figure 4**A). Rho/ROCK agonism and Rac1 inhibition both resulted in decreased *ScxGFP* expression in TGF-β3-treated TPCs, while Rho/ROCK, Cdc42, and myosin inhibition all resulted in increased *ScxGFP* expression (**Figure 4**B-C). Rho/ROCK inhibition resulted in the largest increase in *ScxGFP* expression, but treatment with H1152 limited cell

This article is protected by copyright. All rights reserved.

Author Manuscript

proliferation more than Y27632 treatment (Figure S2, Supplemental Information), so the latter was used in subsequent 2D studies.

To assess the effect of ROCK inhibition on the contractile state of the cell during tenogenic differentiation, identical samples were fixed at day 0, 2, 4 and 6. Rho/ROCK inhibition via Y27632 enhanced *ScxGFP* expression over the course of the study, led to diminished F-actin stress fiber intensity, and almost completely abrogated αSMA production observed in TPCs treated with TGF-β3 only (**Figure 4**D-E). Actin stress fibers terminate at cell-ECM adhesions (i.e., focal adhesions)[32] focal adhesions are typically visualized by the protein vinculin, which is recruited to focal adhesions in a force-dependent manner.[33] Supporting the above observations, the diminished contractile state induced by Rho/ROCK inhibition was substantiated by a reduction in vinculin intensity within focal adhesions despite a consistent number of focal adhesions per cell (**Figure 4**F-H; Figure S3, Supplemental Information). Taken together, these data indicate that TGF-β3 exerts pleiotropic effects on TPCs, inducing proliferation and promoting tenogenesis, but also enhancing contractility, which appears to predispose the cell toward myofibroblastic as opposed to tenogenic differentiation. While there appears to be some tenogenic advantage to using TGF-β3 instead of isoforms 1 or 2 (**Figure 3)**, Rho/ROCK inhibition further potentiates and hinders TGF-β3's tenogenic and pro-myofibroblastic effects, respectively. Previous work has explored the effect of Y27632 treatment in normal human lung fibroblasts, similarly finding that Rho/ROCK inhibition inhibits TGF-β1-mediated myofibroblastic differentiation.[31]

Author Manuscript.

This article is protected by copyright. All rights reserved.

Author Manuscript

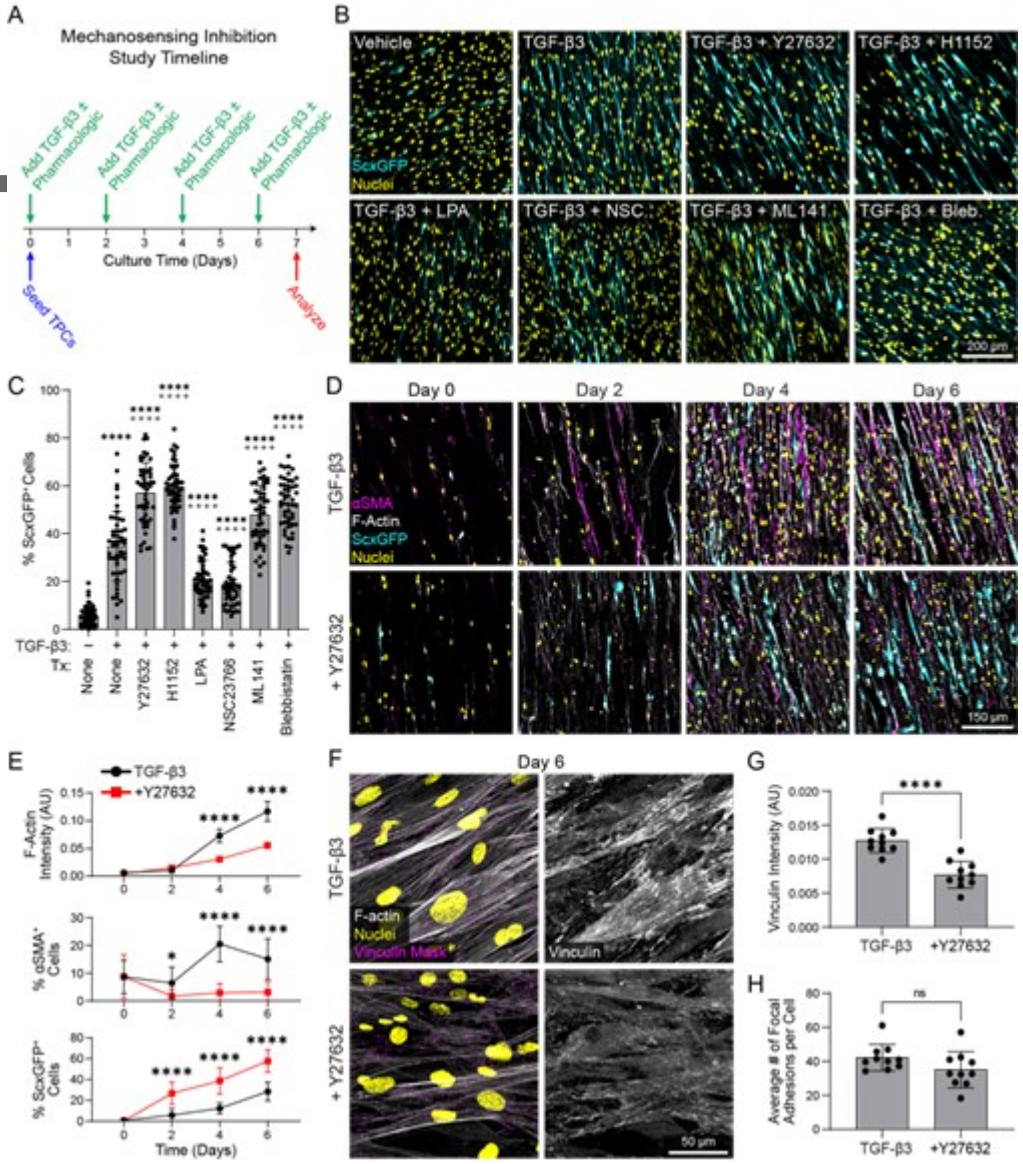


Figure 4 | Rho/ROCK inhibition promotes TGF-β-mediated tenogenesis. A, *ScxGFP* reporter TPCs were cultured for 7 days on aligned fiber-coated coverslips in basal media containing TGF-β3 and supplemented with various pharmacologics targeting Rho GTPase regulators of actin cytoskeleton dynamics or myosin. **B,** Fluorescent images of *ScxGFP* reporter TPCs. **C,** Quantification of % of TPCs expressing *ScxGFP* (n = 50 FOVs, N = 3). Statistical indicators represent comparisons to basal media (*) and media supplemented with TGF-β3 only (+). **D,** Fluorescent images of identical TPC cultures supplemented with TGF-β3 or TGF-β3 and Y27632 (+Y27632), fixed on days 0, 2, 4, and 6; samples were stained for F-actin and αSMA for quantitative analysis. **E,** Quantification of F-actin intensity (AU), % of TPCs expressing *ScxGFP*, and % of TPCs expressing αSMA (n = 25 FOVs, N = 2). **F,** Fluorescent images of TPC cultures fixed on day 6 and stained for vinculin. The binarized vinculin mask denotes focal adhesions and regions within which vinculin intensity was quantified. Quantification of (**G**) vinculin intensity (AU) and (**H**) average number of focal adhesions per cell (n = 10 FOVs). All data are reported as mean ± standard deviation. Asterisks indicate statistically significant comparisons, with ****p<0.0001 by ordinary one- or two-way ANOVA with Tukey's multiple comparisons test or Student's t-test (ns denotes a non-significant comparison).

This article is protected by copyright. All rights reserved.

Author Manuscript

3.5. 3D fiber density and alignment influence spreading and alignment of TPCs but not early tenogenesis

Apart from pharmacologic disruption of actomyosin contractility, myofibroblastic differentiation can also be inhibited by culturing cells on or in soft hydrogel substrates, which is well-known to decrease cell contractility.[34] In previous work, we showed that a DexVS hydrogel crosslinked with an MMP-labile peptide (VPMS) and reinforced with RGD-functionalized DexVS fibers promotes TPC recruitment from a mouse epitenon.[11] Compared to fibronectin- and DexVS fiber-coated glass coverslips (on the order of multiple GPa),[35] FRHCs possess far lower bulk moduli on the order of 0.5-6 kPa.[10a, 17] Anticipating a potential shift in the pleotropic effects of TGF-β in this softer, 3D microenvironment, we re-tested the three TGF-β isoforms for their ability to induce *ScxGFP* expression in TPCs encapsulated in FRHCs with the same crosslinking density as in our previous work (15.0 mM VPMS).[11] Consistent with our prior work, the inclusion of randomly oriented, cell-adhesive (RGD-functionalized) fiber segments in FRHCs enabled contact guidance of encapsulated TPCs, resulting in cells attaining a spindle morphology (**Figure 5**).[11, 36] Similar to our findings on 2D fibrous substrates (**Figure 3**), exogenous addition of TGF-β3 was associated with the greatest increase in *ScxGFP* expression and the smallest increase in αSMA production compared to the vehicle control (**Figure 5**A-B). We also observed a marked decrease in the proportion of αSMA^{+} TPCs in soft, 3D hydrogels as compared to stiff, 2D settings, likely due to the influence of decreased matrix stiffness and dimensionality on cell adhesion and actomyosin contractility, both of which generally are required for myofibroblastic differentiation (**Figures 3**E, **5**B).[17, 34] TGF-β3 was the least fibrotic of the three isoforms in this *in vitro* model and was therefore used in the subsequent studies. However, TGF-β1 signaling is known to exhibit different downstream transcriptional effects in regenerative (MRL-MpJ) vs. fibrotic (adult C57BL/6) tendon healing environments, where C57BL/6 tendons show positively-enriched inflammatory and fibrotic pathways.[4e] Future work should therefore assess the broader transcriptional profiles of TPCs as a function of exposure to different isoforms of TGF-β.

To study the role of fibrous topographical alignment in tenogenesis in 3D, we developed a microfluidic chip capable of flow-aligning fiber segments, resulting in FRHCs with distinct domains possessing non-aligned or aligned fibers. Independent of fiber

This article is protected by copyright. All rights reserved.

alignment, TPCs consistently contact-guided along embedded fibers to achieve uniaxial, spindle morphologies, but at a population level, adopted an orientation reflecting global fiber alignment (**Figure 5**C). Surprisingly, neither fiber density nor alignment influenced *ScxGFP* expression of encapsulated TPCs (**Figure 5**D-E). Although fiber anisotropy in flow-aligned FRHCs increased marginally with fiber density, all fiber densities tested were significantly more aligned than randomly oriented fibers at 2.5 v/v% (Figure S4D-F, Supplemental Information). A potential explanation for the disparate influences of fiber alignment in 2D vs. 3D may lie in the difference between how TPCs engage adhesive fibers across these two settings. While TPCs on 2D fibrous substrates engage multiple fibers simultaneously, thereby disrupting their spindle morphology on randomly oriented substrates, TPCs in 3D FHRCs typically engaged only a single fiber, regardless of overall fiber alignment. As such, TPC in FHRCs consistently achieved a spindle morphology whether encapsulated fibers were collectively aligned or disorganized. These observations further support the notion that a spindle morphology is a pro-tenogenic cytoskeletal state for TPCs, but they also suggest that tenogenesis is not influenced by the collective organization of TPCs.

MMP-labile crosslink density influences hydrogel stiffness but also modulates cell spreading kinetics in 3D,[37] and so we additionally screened crosslinking density for its effect on TPC morphology and *ScxGFP* expression. We noted a TGF-β3-mediated increase in nuclear ScxGFP intensity in FHRCs crosslinked with 17.5 mM compared to 12.5 mM VPMS; however, heightened crosslinking also resulted in diminished spreading of the TPCs, motivating the use of a crosslinker concentration of 15.0 mM for all subsequent 3D studies (Figure S4, Supplemental Information). With heterogeneous spreading noted across the crosslinking densities tested in this study, readouts of cytosolic ScxGFP intensity were likely confounded, and so this design decision was based primarily on nuclear ScxGFP intensity.

Author Manuscript

This article is protected by copyright. All rights reserved.

Author Manuscript

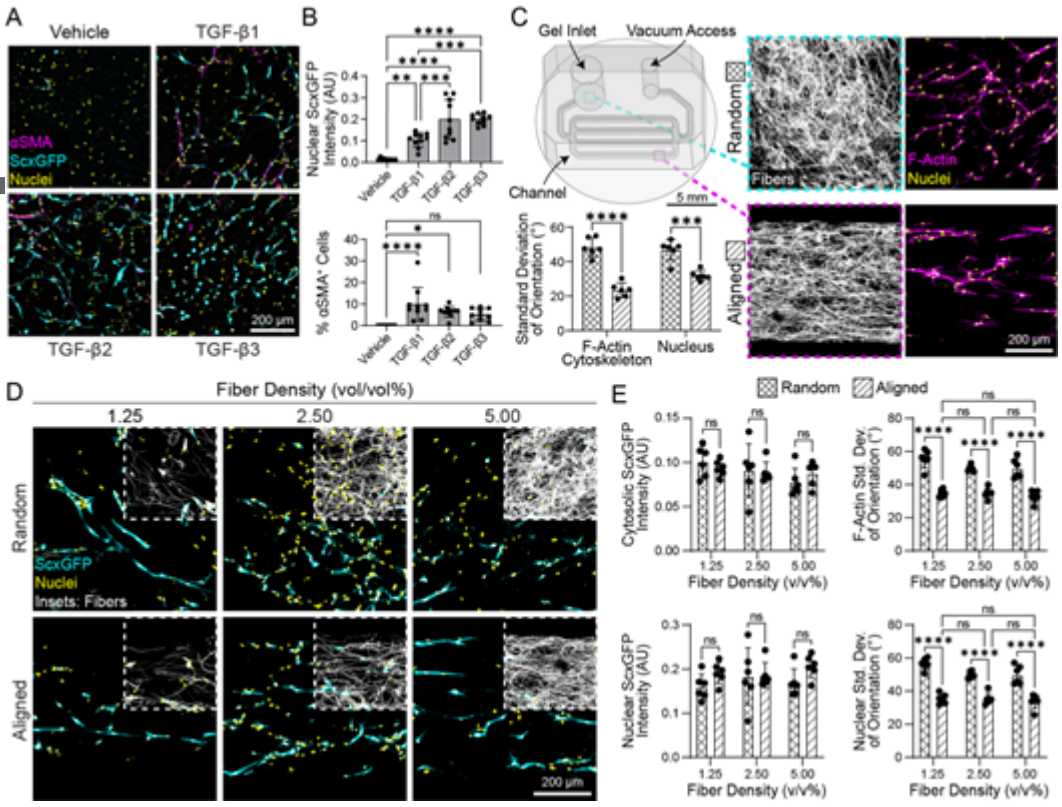


Figure 5 | TPC spreading and tenogenesis in fiber-reinforced hydrogel composites (FRHCs) with tunable topographical anisotropy. A, Fluorescent images of *ScxGFP* reporter TPCs encapsulated in DexVS FRHCs and cultured for 7 days in basal media or supplemented with various isoforms of TGF-β. **B,** Quantification of nuclear ScxGFP intensity (AU) and % of cells expressing αSMA (n = 10 FOVs). **C,** Schematic of microfluidic flow-alignment device used to generate FRHCs with anisotropic fibrous topography. Fluorescent images of fibers and TPCs fixed after 7 days of culture in random and flow-aligned regions of the device. Quantification of standard deviation of orientation (°) of TPC cytoskeletons and nuclei (n = 6 FOVs). **D,** Fluorescent images of TPCs cultured for 7 days with TGF-β3 in DexVS FRHCs with varying fiber density and alignment. **E,** Quantification of nuclear and cytosolic ScxGFP intensity (AU) in addition to the standard deviation of orientation (°) of TPC cytoskeletons and nuclei (n = 6 FOVs, N = 3). All data are reported as mean ± standard deviation. Asterisks indicate statistically significant comparisons, with *p<0.05, **p<0.01, ***p<0.001, and ****p<0.0001 by ordinary one- or two- way ANOVA with Tukey's multiple comparisons test (ns denotes a non-significant comparison).

3.6. Inhibition of cell contractility potentiates tenogenesis in 3D microenvironments

To confirm the pro-tenogenic influence of Rho/ROCK inhibition identified in our earlier 2D studies (**Figure 4**B-C) on *ScxGFP* expression in 3D, TPCs in aligned FHRCs were treated with TGF-β3, Y27632, or both over the course of one week. Y27632 dosing was screened again in 3D, and 10 μM was found to yield a more consistent increase in *ScxGFP* expression compared to the 30 μM dose employed in 2D studies (**Figure 6**A-B; Figure S5, Supplemental Information). While *ScxGFP* expression was primarily driven by TGF-β3, Rho/ROCK inhibition

This article is protected by copyright. All rights reserved.

Author Manuscript

via Y27632 resulted in an additional, albeit marginal increase in *ScxGFP* expression that was most prominent intranuclearly (**Figure 6**A-B). We speculate that there may be biological significance to this apparent nuclear localization given the role of Scleraxis as a transcription factor, but future work is needed to delineate the roles of nuclear vs. cytoplasmic Scleraxis as it pertains to tenogenic differentiation. Screening the same panel of canonical tenogenic genes as in 2D studies (**Figure 1**), we found that exogenous TGF-β3 addition to Rho/ROCK-inhibited TPCs resulted in marked upregulation of *Scx*, *Tnmd*, *Tnc*, *Mkx*, *Fmod*, *Bgn*, *Dcn*, and *Col1a2*, indicating more robust tenogenesis of TPCs in FRHCs as compared culture on 2D substrates (**Figure 6**C). Moreover, Rho/ROCK inhibition limited TGF- β3-driven expression of *Acta2*, the gene encoding αSMA. We hypothesize that the combined influences of a softer microenvironment and Rho/ROCK inhibition better promote tenogenesis over myofibroblastic differentiation. Dimensionality may also play a role in this fate switch because, in contrast to 2D cultures, 'substrate stiffness' in 3D cultures is related to crosslinking density, which is at the same time inhibitory to cell spreading and myofibroblastic differentiation.[17]

This article is protected by copyright. All rights reserved.

Author Manuscript

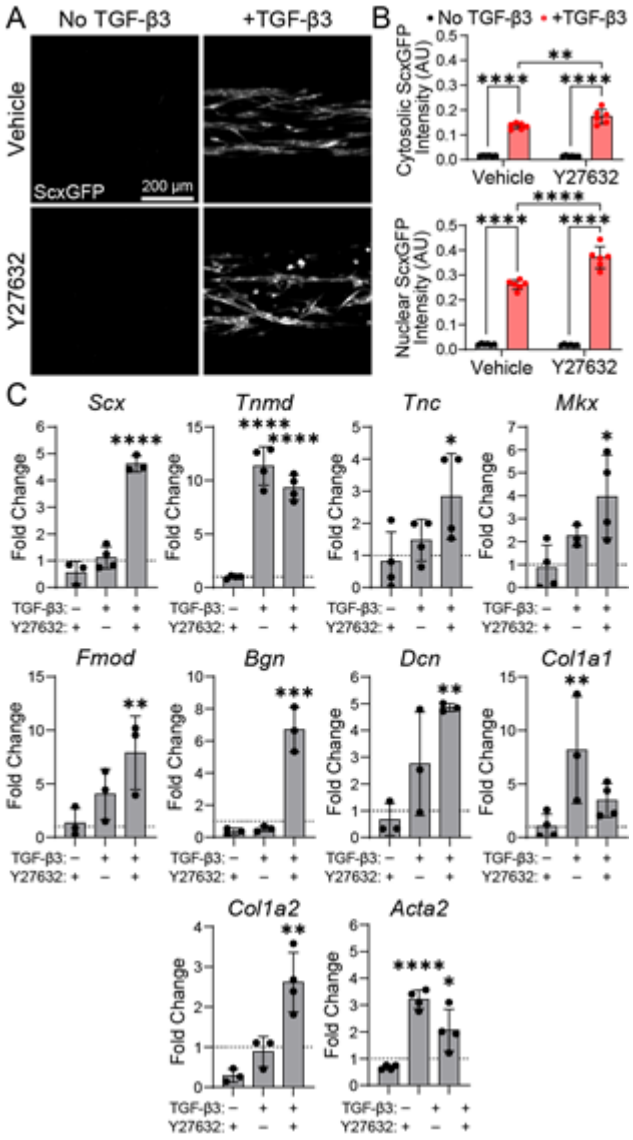


Figure 6 | Rho/ROCK inhibition potentiates TGF-β-mediated tenogenesis in 3D. A, Fluorescent images of *ScxGFP* reporter TPCs encapsulated in flow-aligned FRHCs and cultured for 7 days in basal media or supplemented with Y27632, TGF-β3, or both. **B,** Quantification of cytosolic and nuclear ScxGFP intensity (AU) (n = 6 FOVs, N = 2). **C,** Fold change in expression of canonical tenogenic genes by TPCs encapsulated in FRHCs and treated with Y27632, TGF-β3, or a combination for 7 days (n = 3 cultures, N = 2). A fold change of 1 is denoted with a black, dotted line. All data are reported as mean ± standard deviation. Asterisks indicate statistically significant comparisons, with *p<0.05, **p<0.01, ***p<0.001, and ****p<0.0001 by ordinary one- (soluble condition) or two-way (TGF-β3 treatment, Y27632 treatment) ANOVA with Tukey's multiple comparisons test.

3.7. Topographical alignment templates de novo matrix production

While fiber orientation in 3D did not impact tenogenesis over short-term, 1 week-long studies (**Figure 5**), we hypothesized that topographical anisotropy may yet influence long-term maintenance of the tenogenic phenotype and the organization of *de novo* collagen synthesized by differentiated TPCs. Therefore, we performed 4-week studies

This article is protected by copyright. All rights reserved.

examining the effect of TGF-β3 treatment as a function of fiber alignment on TPC tenogenesis and matrix deposition in FHRCs. Similar to observations at 1 week, heightened *ScxGFP* expression was driven only by TGF-β3 treatment and remained insensitive to fiber alignment (**Figure 7**A-D).

A critical outcome of robust tenogenesis in the context of tendon healing is the deposition of aligned collagen fibrils capable of bearing the tensile loads required of tendons. Matrix organization is particularly important, as this is a major delineator between functional tendon and scar tissue, both of which are predominantly composed of type I collagen.[3b, 3c, 38] Moreover, with *Dcn*, *Tnc*, and *Col1a1* all being heavily implicated in fibrosis in other organs,[39] maturity and organization of *de novo* collagen fibrils represents a critical feature of tendon healing. To assess these more salient outcomes, cryosections from FHRCs cultured for 4 weeks were stained with Picrosirius Red to visualize fibrillar collagens, providing a measure of collagen content, but also a measure of the maturity and alignment of the collagen fibrils via birefringence imaged under polarized light.[40] Picrosirius Red staining showed that topographical alignment had no effect on the amount of collagen deposited but drastically improved the maturity (i.e., fibril size and intra-fibrillar crosslinking) and alignment of *de novo* collagen fibrils, as measured by birefringence under polarized light (**Figure 7**E-H). Collagen content showed a dose-dependent relationship with fiber density, with composites containing 2.5 v/v% fibers achieving ~60% collagen by weight (**Figure 7**I-K); this is notable given that native tendon is 60-85% collagen by weight.[38a, 41] *De novo* collagen fibrils showed increased maturity and alignment with increasing fiber density, but this relationship reversed above 2.5 v/v% (**Figure 7**L). This diminishing return in *de novo* collagen maturity and organization with respect to synthetic fiber density could be attributed to TPC engagement to multiple fibers, which may confound cell alignment as compared to engagement to fewer fibers.[36, 42] This phenomenon may be akin to our observations in 2D, where engagement to abundant, randomly oriented fibers disrupted TPCs' ability to achieve a spindle morphology (**Figure 2**C).

This article is protected by copyright. All rights reserved.

Author Manuscript

Author Manuscript

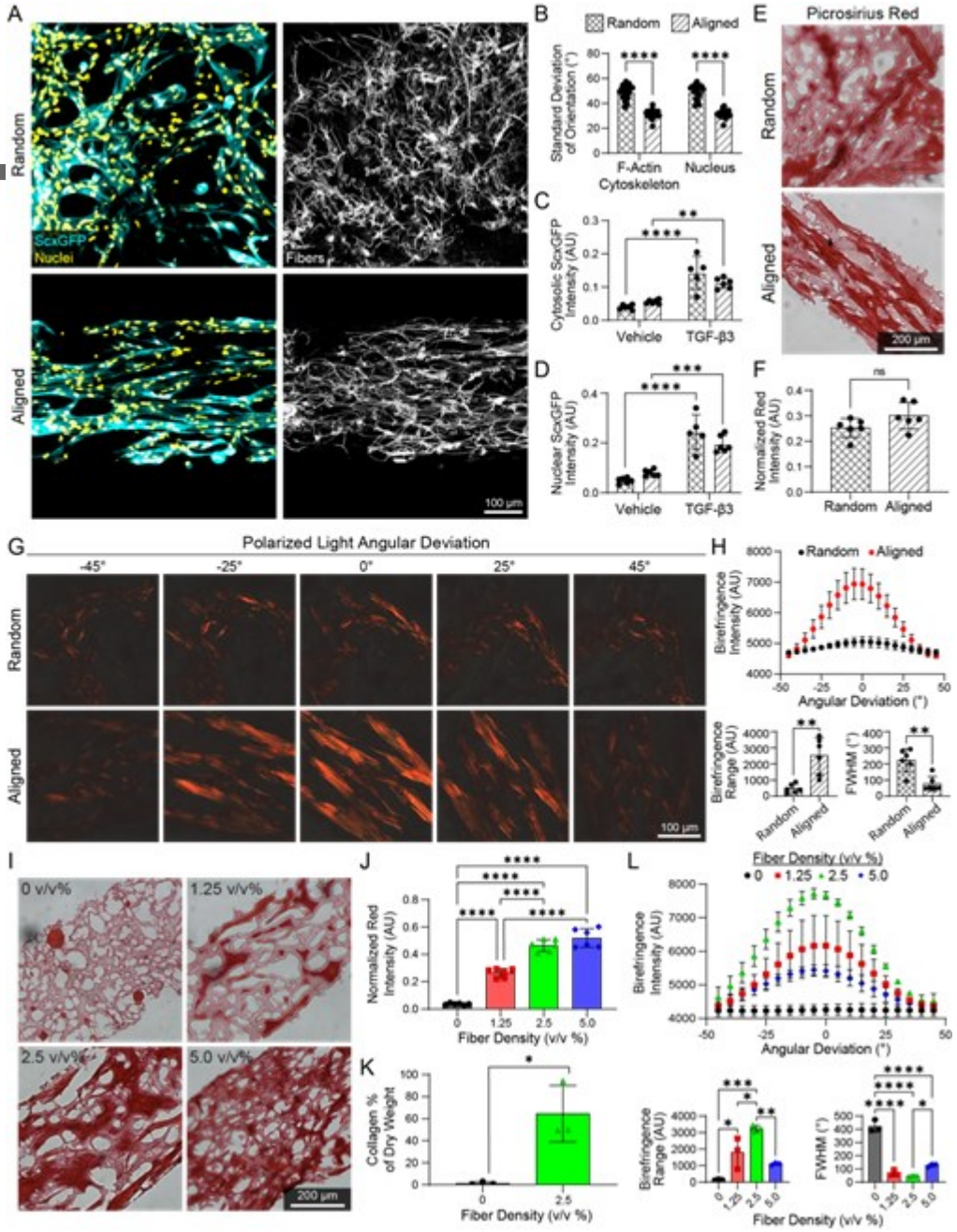


Figure 7 | 3D aligned fibrous topography templates *de novo* collagen deposition in FHRCs. A, Fluorescent images of *ScxGFP* reporter TPCs encapsulated in FRHCs with varying fiber alignment and cultured for 4 weeks with TGF-β3. Quantification of (**B**) standard deviation of orientation (°) of TPC cytoskeletons and nuclei, (**C**) cytosolic ScxGFP intensity, and (**D**) nuclear ScxGFP intensity (n = 6 FOVs, N = 2). **E,** Brightfield images of Picrosirius Red-stained frozen sections of 4-week TPC cultures in random and aligned FRHCs. **F,** Quantification of normalized red intensity (AU) (n = 6 FOVs, N = 2). **G,** Polarized light images of random and aligned 4-week FRHC cultures over a range of angular deviation. **H,** Quantification of birefringence intensity (AU) as a function of angular deviation (°), birefringence range (AU), and full width at half maximum (°) (n = 6 FOVs, N = 2). **I,** Brightfield images of Picrosirius Red-stained sections of 4-week TPC cultures in flow-aligned FRHCs with varying fiber density. Quantification of (**J**) normalized red intensity (AU) (n = 6 FOVs), (**K**) collagen % dry weight (n = 3 hydrogels), and (**L**) birefringence intensity (AU) as a function of angular deviation (°), birefringence range (AU), and full width at half maximum (FWHM) (°) (n = 3 FOVs). All data are reported as mean ± standard deviation. Asterisks indicate statistically significant comparisons, with

This article is protected by copyright. All rights reserved.

*p<0.5, **p<0.01, ***p<0.001, and ****p<0.0001 by ordinary one- or two-way ANOVA with Tukey's multiple comparisons test or Student's t-test (ns denotes a non-significant comparison).

Author Manuscript

3.8. Tenogenesis of human tendon-derived cells in FRHCs is donor-dependent

To assess the translatability of our material design parameters derived from murine TPCs, we isolated tendinopathic TDCs from human donors and cultured them in the conditions optimized above. The average age of these patients was 57 ± 6.6 years (range: 50-63 years; all female), which is within the typical age range of patients presenting with insertional Achilles tendinitis or biceps tendinopathy associated with rotator cuff disease (**Figure 8**A).[43] For Donors 1 and 2 (Achilles), portions of the tissue sample were sectioned and stained with Hematoxylin and Eosin to obtain Bonar tendinopathy scores of 4 and 9, respectively, suggesting that TDCs from Donor 2 originated from a more tendinopathic environment than those from Donor 1 (Figure S7, Supplemental Information). A tendinopathy score for Donor 3's tissue was not obtained (**Figure 8**A), but this patient had a diagnosis of chronic biceps tendinopathy that was confirmed intraoperatively.

To assess the effects of TGF-β3 and cytoskeletal contractility on early tenogenesis of human TDCs in FRHCs, TDCs from each donor were cultured in fibrous (2.5 v/v%) DexVS hydrogels for 1 week, supplemented either with TGF-β3 or a combination of TGF-β3 and Y27632. With combined TGF-β3 treatment and Rho/ROCK inhibition, while TDCs from Donor 1 showed positive fold changes in MKX, TNC, TNMD, and COL1A1, Donor 2 generally showed no change in expression of these genes, and Donor 3 exhibited significant downregulation of TNC, TNMD, and COL3A1 (**Figure 8**B). Overall, none of the three TDC populations upregulated canonical tenogenic genes to the same extent as murine TPCs (**Figure 6**C, **8**B). Interestingly, TDCs did not exhibit increased ACTA2 expression in response to TGF-β3 stimulation, potentially indicating that these TDCs are relatively senescent compared to the murine TPCs.

To evaluate deposition and organization of *de novo* collagen, samples were cultured in flow-aligned FRHCs (2.5 v/v% fibers) for 2-4 weeks with or without TGF-β3 supplementation. 3D cultures from Donors 1 and 2 began to contract away from the underlying glass substrate at 2 weeks, and so they were fixed in paraformaldehyde at that

This article is protected by copyright. All rights reserved.

timepoint while Donor 3's culture was able to proceed to 4 weeks without issue. At their endpoints, frozen sections of FRHCs were stained with Picrosirius Red (**Figure 8**C). Intuitively, TGF-β3 treatment resulted in increased collagen deposition by TDCs from Donors 1 and 2. However, Donor 3's culture did not respond with increased collagen deposition with TGF-β3 treatment compared to vehicle controls (**Figure 8**C-D). The maturity and organization of *de novo* collagen was reflected via birefringence under polarized light in cultures from Donors 1 and 2, which showed greater birefringence intensity and dependence on sample orientation compared to that of Donor 3 (**Figure 8**E-F). TDCs also exhibited heightened αSMA and F-actin intensities via immunofluorescence in response to TGF-β3, implying myofibroblastic differentiation in all three donor cultures. A shift toward this myofibroblastic phenotype was most prominent in cultures from Donor 3 (Figure S8, Supplemental Information). Taken together, these results demonstrate that the regenerative capacity of human TDCs varies as a function of donor source (i.e., patient, disease progression, and anatomical location). Epitenon-derived progenitor populations are known to contribute to both fibrotic and regenerative healing in humans, where the former population is characterized by enrichment of pro-fibrotic and pro-inflammatory genes.[5a] With increasing severity of chronic inflammation, this progenitor pool may become depleted or biased toward a pro-fibrotic or senescent phenotype, precluding tenogenesis and limiting deposition of mature, aligned collagen fibrils during healing.

Author Manuscript

This article is protected by copyright. All rights reserved.

Author Manuscript

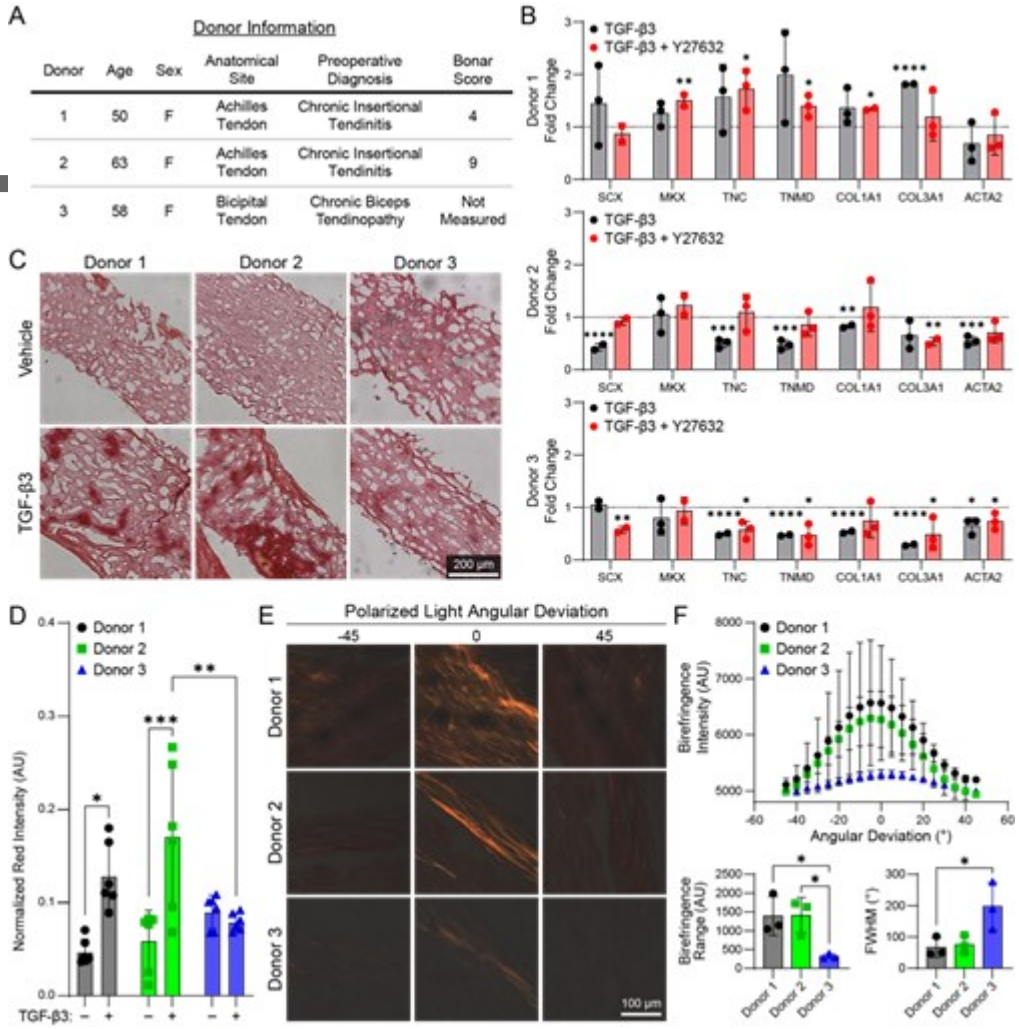


Figure 8 | Human TDCs exhibit variable capacity for tenogenesis and organized collagen deposition. A, Demographic information and Bonar tendinopathy scores for 3 tendon tissue donors from whom human TDCs were isolated. **B,** Fold change in expression of canonical tenogenic genes by TDCs encapsulated in FRHCs and treated with TGF-β3 or a combination of TGF-β3 and Y27632 for 7 days (n = 3 hydrogels). A fold change of 1 is denoted with a black, dotted line. **C,** Brightfield images of Picrosirius Red-stained frozen sections of 2- (Donors 1 and 2) and 4-week (Donor 3) TDC cultures in flow-aligned FRHCs. **D,** Quantification of normalized red intensity (AU) (n = 6 FOVs). **E,** Polarized light images of aligned 2-4-week FRHC cultures with TGF-β3 over a range of angular deviation. **F,** Quantification of birefringence intensity (AU) as a function of angular deviation (°), birefringence range (AU), and full width at half maximum (FWHM) (°) (n = 3 FOVs). All data are reported as mean ± standard deviation. Asterisks indicate statistically significant comparisons, with *p<0.05, **p<0.01, ***p<0.001, and ****p<0.0001 by ordinary one- or two-way ANOVA with Tukey's multiple comparisons test.

4. *CONCLUSION*

Here, we applied a combination of 2D and 3D engineered culture platforms to identify the salient physical and biochemical cues driving tenogenic differentiation and

This article is protected by copyright. All rights reserved.

organized matrix deposition by murine TPCs and human TDCs. This work highlights a tenogenic vs. myofibroblastic fate switch as a function of TGF-β isoform, where TGF-β3 treatment, softer substrates, and actin cytoskeletal dysregulation by Rho/ROCK inhibition led to more complete tenogenic differentiation. While an aligned, fibrous topography drove tenogenesis of individualized TPCs in 2D, the impact of fiber alignment in 3D FRHCs was limited to the organization of *de novo* collagenous matrix, delineating the roles of cell spreading morphology and cellular organization in tenogenic differentiation and matrix remodeling, respectively. These findings inform design parameters of cell-free, injectable, synthetic hydrogels for tendon tissue regeneration. Finally, we showed that human TDCs exhibit heterogeneity with respect to their tenogenesis and matrix synthesis in response to TGF-β3. Cell-free therapies that depend on recruitment of endogenous progenitors will therefore require a better understanding of the pathways regulating a pro-fibrotic vs. pro-regenerative phenotype in these cell populations to uncover novel therapeutic targets. For example, next-generation FRHCs could modulate the soluble milieu to prime the immune response toward an M2-like phenotype, which is known to yield a more pro-regenerative tendon healing response.[4g, 44] Future work will therefore explore the effects of FRHC injection on TPC and immune cell recruitment, immune phenotype polarization, tenogenic differentiation of TPCs, and functional tendon regeneration in a murine Achilles tendon injury model.

ACKNOWLEDGMENTS

Ronen Schweitzer kindly provided the *ScxGFP* reporter mouse line used in this work. Paul G. Talusan (P.G.T.) generously provided human Achilles tendon tissue. R.N.K. acknowledges financial support from the National Institute of Dental & Craniofacial Research of the National Institutes of Health Tissue Engineering at Michigan T32 Training Grant (T32DE00705745); he also acknowledges financial support from the National Institute of Arthritis and Musculoskeletal and Skin Diseases (NIAMS) of the Ruth L. Kirschstein National Research Service Award (NRSA) Individual Predoctoral Fellowship (Parent F31 AR082308). M.E.J. and L.A.H. acknowledge financial support from the National Science Foundation (NSF) Graduate Research Fellowship Program (DGE2241144). The authors acknowledge support for this work from the Michigan Integrative Musculoskeletal Health

This article is protected by copyright. All rights reserved.

Author Manuscript

Core Center, which is a NIAMS Resource-based Center for Bone, Muscle, and Orthopaedic Research (P30 AR069620). The also authors acknowledge financial support of the University of Michigan Medical School and College of Engineering and the University of Michigan Endowment for Basic Sciences.

AUTHOR CONTRIBUTIONS

R.N.K., E.A.C., M.L.K., A.C.A., A.S., A.H.H, and B.M.B designed the experiments. R.N.K., E.A.C., A.C.A, and B.M.B. contributed to IRB protocols enabling harvest of human bicipital and Achilles tendon tissue. E.A.C. harvested human bicipital and Achilles tendon tissue. A.C.A. contributed to the TPC isolation protocol. R.N.K, T.P.B., and M.S. contributed to substrate fabrication, *in vitro* studies, and analyses thereof. M.E.J. contributed to the design of the flow-alignment device. L.A.H. and A.C.A. isolated human TDCs from Achilles tendon tissue, and L.A.H., A.C.A., and M.L.K. processed tissues for paraffin histology. R.N.K. and B.M.B. wrote the manuscript. All authors reviewed the manuscript.

COMPETING INTERESTS

The authors declare that they have no known competing financial interests or personal relationships that could appear to have influenced the work reported in this paper.

REFERENCES

[1] a) A. Praemer, S. Furner, D. P. Rice, *Musculoskeletal Conditions in the United States*, American Academy of Orthopedic Surgeons, **1999**; b) *United States Bone and Joint Initiative: The Burden of Musculoskeletal Disease in the United States, Fourth Edition*, American Academy of Orthopedic Surgeons, **2016**; c) N. J. Lemme, N. Y. Li, S. F. DeFroda, J. Kleiner, B. D. Owens, *Orthop J Sports Med* **2018**, 6, 2325967118808238.

[2] a) I. Lantto, J. Heikkinen, T. Flinkkila, P. Ohtonen, P. Siira, V. Laine, J. Leppilahti, *Am J Sports Med* **2016**, 44, 2406; b) K. Nilsson-Helander, K. G. Silbernagel, R. Thomee, E. Faxen, N. Olsson, B. I. Eriksson, J. Karlsson, *Am J Sports Med* **2010**, 38, 2186.

[3] a) M. L. Killian, L. Cavinatto, L. M. Galatz, S. Thomopoulos, *J Shoulder Elbow Surg* **2012**, 21, 228; b) F. Wu, M. Nerlich, D. Docheva, *EFORT Open Rev* **2017**, 2, 332; c) P. Sharma, N. Maffulli, *J Musculoskelet Neuronal Interact* **2006**, 6, 181.

[4] a) K. Howell, C. Chien, R. Bell, D. Laudier, S. F. Tufa, D. R. Keene, N. Andarawis-Puri, A. H. Huang, *Sci Rep* **2017**, 7, 45238; b) T. Sakabe, K. Sakai, T. Maeda, A. Sunaga, N. Furuta, R. Schweitzer, T. Sasaki, T. Sakai, *J Biol Chem* **2018**, 293, 5766; c) K. T. Best, A. E. Loiselle, *FASEB J* **2019**, 33, 8578; d) N. S. George, R. Bell, J. J. Paredes, P. J. Taub, N. Andarawis-Puri, *J Orthop Res* **2021**, 39, 1344; e) J. G. Kallenbach, M. A. T. Freeberg, D. Abplanalp, R. G. Alenchery, R. E. Ajalik, S. Muscat, J. A. Myers, J. M. Ashton, A. Loiselle, M. R. Buckley, A. J. van Wijnen, H. A. Awad, *Sci Rep* **2022**, 12, 3026; f) D. A. Kaji, K. L. Howell, Z. Balic, D. Hubmacher, A. H. Huang,

This article is protected by copyright. All rights reserved.

Author Manuscript

Author Manuscript

Elife **2020**, 9; g) V. Arvind, K. Howell, A. H. Huang, *BioRxiv* **2021**, DOI: 10.1101/2021.05.12.443424.

[5] a) A. E. C. Nichols, N. W. Wagner, C. Ketonis, A. E. Loiselle, *bioRxiv* **2023**, DOI: 10.1101/2023.01.30.526242; b) B. Walia, A. H. Huang, *J Orthop Res* **2019**, 37, 1270.

[6] a) R. J. de Vos, A. Weir, H. T. van Schie, S. M. Bierma-Zeinstra, J. A. Verhaar, H. Weinans, J. L. Tol, *JAMA* **2010**, 303, 144; b) W. M. Efird, A. G. Fletcher, R. W. Draeger, J. T. Spang, L. E. Dahners, P. S. Weinhold, *Orthop J Sports Med* **2018**, 6, 2325967118802792; c) H. Tempfer, A. Kaser-Eichberger, C. Lehner, R. Gehwolf, S. Korntner, N. Kunkel, A. Wagner, M. Gruetz, L. M. Heindl, F. Schroedl, A. Traweger, *Cell Physiol Biochem* **2018**, 46, 1148; d) S. Tarafder, C. Ricupero, S. Minhas, R. J. Yu, A. D. Alex, C. H. Lee, *Theranostics* **2019**, 9, 4241.

[7] a) S. Font Tellado, E. R. Balmayor, M. Van Griensven, *Adv Drug Deliv Rev* **2015**, 94, 126; b) B. M. Baker, R. P. Shah, A. M. Silverstein, J. L. Esterhai, J. A. Burdick, R. L. Mauck, *Proc Natl Acad Sci U S A* **2012**, 109, 14176; c) B. M. Baker, R. L. Mauck, *Biomaterials* **2007**, 28, 1967.

[8] a) J. Cai, J. Liu, J. Xu, Y. Li, T. Zheng, T. Zhang, K. Han, S. Chen, J. Jiang, S. Wu, J. Zhao, *Biofabrication* **2023**, 15; b) J. L. Koh, Z. Szomor, G. A. Murrell, R. F. Warren, *Am J Sports Med* **2002**, 30, 410; c) A. English, A. Azeem, K. Spanoudes, E. Jones, B. Tripathi, N. Basu, K. McNamara, S. A. M. Tofail, N. Rooney, G. Riley, A. O'Riordan, G. Cross, D. Hutmacher, M. Biggs, A. Pandit, D. I. Zeugolis, *Acta Biomater* **2015**, 27, 3; d) Y. J. No, M. Castilho, Y. Ramaswamy, H. Zreiqat, *Adv Mater* **2020**, 32, e1904511; e) A. Islam, T. Mbimba, M. Younesi, O. Akkus, *Acta Biomater* **2017**, 58, 244.

[9] a) S. Testa, M. Costantini, E. Fornetti, S. Bernardini, M. Trombetta, D. Seliktar, S. Cannata, A. Rainer, C. Gargioli, *J Cell Mol Med* **2017**, 21, 2711; b) Y. Wang, S. Jin, D. Luo, D. He, C. Shi, L. Zhu, B. Guan, Z. Li, T. Zhang, Y. Zhou, C. Y. Wang, Y. Liu, *Nat Commun* **2021**, 12, 1293; c) B. P. Purcell, D. Lobb, M. B. Charati, S. M. Dorsey, R. J. Wade, K. N. Zellars, H. Doviak, S. Pettaway, C. B. Logdon, J. A. Shuman, P. D. Freels, J. H. Gorman, 3rd, R. C. Gorman, F. G. Spinale, J. A. Burdick, *Nat Mater* **2014**, 13, 653.

[10] a) D. L. Matera, W. Y. Wang, M. R. Smith, A. Shikanov, B. M. Baker, *ACS Biomat Sci Eng* **2019**, 5, 2965; b) H. L. Hiraki, D. L. Matera, M. J. Rose, R. N. Kent, C. W. Todd, M. E. Stout, A. E. Wank, M. C. Schiavone, S. J. DePalma, A. A. Zarouk, B. M. Baker, *Front Bioeng Biotechnol* **2021**, 9, 679165.

[11] R. N. Kent, M. Said, M. E. Busch, E. R. Poupard, A. Tsai, J. Xia, D. L. Matera, W. Y. Wang, S. J. DePalma, H. L. Hiraki, M. L. Killian, A. C. Abraham, J. W. Shin, A. H. Huang, A. Shikanov, B. M. Baker, *Adv Funct Mater* **2022**, 32.

[12] a) A. H. Huang, H. H. Lu, R. Schweitzer, *J Orthop Res* **2015**, 33, 800; b) R. Schweitzer, J. H. Chyung, L. C. Murtaugh, A. E. Brent, V. Rosen, E. N. Olson, A. Lassar, C. J. Tabin, *Development* **2001**, 128, 3855; c) H. Liu, J. Xu, Y. Lan, H. W. Lim, R. Jiang, *Front Cell Dev Biol* **2021**, 9, 654397.

[13] G. K. Tan, B. A. Pryce, A. Stabio, J. V. Brigande, C. Wang, Z. Xia, S. F. Tufa, D. R. Keene, R. Schweitzer, *Elife* **2020**, 9.

[14] A. Shimada, S. Wada, K. Inoue, H. Ideno, T. Kamiunten, K. Komatsu, A. Kudo, Y. Nakamura, T. Sato, K. Nakashima, A. Nifuji, *Histochem Cell Biol* **2014**, 142, 205.

[15] Y. Bi, D. Ehirchiou, T. M. Kilts, C. A. Inkson, M. C. Embree, W. Sonoyama, L. Li, A. I. Leet, B. M. Seo, L. Zhang, S. Shi, M. F. Young, *Nat Med* **2007**, 13, 1219.

[16] Y. Yu, Y. Chau, *Biomacromolecules* **2012**, 13, 937.

[17] D. L. Matera, K. M. DiLillo, M. R. Smith, C. D. Davidson, R. Parikh, M. Said, C. A. Wilke, I. M. Lombaert, K. B. Arnold, B. B. Moore, B. M. Baker, *Sci Adv* **2020**, 6.

[18] R. L. Mauck, X. Yuan, R. S. Tuan, *Osteoarthritis Cartilage* **2006**, 14, 179.

[19] H. Stegemann, K. Stalder, *Clin Chim Acta* **1967**, 18, 267.

[20] R. E. Neuman, M. A. Logan, *J Biol Chem* **1950**, 184, 299.

[21] A. Fearon, J. E. Dahlstrom, J. Twin, J. Cook, A. Scott, *J Sci Med Sport* **2014**, 17, 346.

This article is protected by copyright. All rights reserved.

Author Manuscript

[22] P. Bankhead, M. B. Loughrey, J. A. Fernandez, Y. Dombrowski, D. G. McArt, P. D. Dunne, S. McQuaid, R. T. Gray, L. J. Murray, H. G. Coleman, J. A. James, M. Salto-Tellez, P. W. Hamilton, *Sci Rep* **2017**, 7, 16878.
[23] B. A. Pryce, A. E. Brent, N. D. Murchison, C. J. Tabin, R. Schweitzer, *Dev Dyn* **2007**, 236, 1677.
[24] a) I. Rajpar, J. G. Barrett, *J Tissue Eng* **2019**, 10, 2041731419848776; b) S. Tarafder, J. A. Brito, S. Minhas, L. Effiong, S. Thomopoulos, C. H. Lee, *Biofabrication* **2019**, 12, 015008; c) T. Harvey, S. Flamenco, C. M. Fan, *Nat Cell Biol* **2019**, 21, 1490; d) C. H. Lee, F. Y. Lee, S. Tarafder, K. Kao, Y. Jun, G. Yang, J. J. Mao, *J Clin Invest* **2015**, 125, 2690; e) K. Kashiwagi, Y. Mochizuki, Y. Yasunaga, O. Ishida, M. Deie, M. Ochi, *Scand J Plast Reconstr Surg Hand Surg* **2004**, 38, 193.
[25] a) Z. Yin, X. Chen, J. L. Chen, W. L. Shen, T. M. Hieu Nguyen, L. Gao, H. W. Ouyang, *Biomaterials* **2010**, 31, 2163; b) V. Kishore, W. Bullock, X. Sun, W. S. Van Dyke, O. Akkus, *Biomaterials* **2012**, 33, 2137; c) J. Zhu, J. Li, B. Wang, W. J. Zhang, G. Zhou, Y. Cao, W. Liu, *Biomaterials* **2010**, 31, 6952.
[26] Y. Li, X. Liu, X. Liu, Y. Peng, B. Zhu, S. Guo, C. Wang, D. Wang, S. Li, *Growth Factors* **2022**, 40, 98.
[27] D. Park, E. Wershof, S. Boeing, A. Labernadie, R. P. Jenkins, S. George, X. Trepat, P. A. Bates, E. Sahai, *Nat Mater* **2020**, 19, 227.
[28] C. Stoll, T. John, M. Endres, C. Rosen, C. Kaps, B. Kohl, M. Sittinger, W. Ertel, G. Schulze-Tanzil, *J Orthop Res* **2010**, 28, 1170.
[29] a) P. J. Wipff, D. B. Rifkin, J. J. Meister, B. Hinz, *J Cell Biol* **2007**, 179, 1311; b) P. B. Voleti, M. R. Buckley, L. J. Soslowsky, *Annu Rev Biomed Eng* **2012**, 14, 47; c) C. N. Manning, H. M. Kim, S. Sakiyama-Elbert, L. M. Galatz, N. Havlioglu, S. Thomopoulos, *J Orthop Res* **2011**, 29, 1099.
[30] N. Sandbo, N. Dulin, *Transl Res* **2011**, 158, 181.
[31] D. L. Matera, A. T. Lee, H. L. Hiraki, B. M. Baker, *Cell Mol Bioeng* **2021**, 14, 381.
[32] a) M. Abercrombie, J. E. Heaysman, S. M. Pegrum, *Exp Cell Res* **1971**, 67, 359; b) K. Burridge, K. Fath, T. Kelly, G. Nuckolls, C. Turner, *Annu Rev Cell Biol* **1988**, 4, 487.
[33] a) C. Grashoff, B. D. Hoffman, M. D. Brenner, R. Zhou, M. Parsons, M. T. Yang, M. A. McLean, S. G. Sligar, C. S. Chen, T. Ha, M. A. Schwartz, *Nature* **2010**, 466, 263; b) A. Carisey, R. Tsang, A. M. Greiner, N. Nijenhuis, N. Heath, A. Nazgiewicz, R. Kemkemer, B. Derby, J. Spatz, C. Ballestrem, *Curr Biol* **2013**, 23, 271.
[34] X. Huang, N. Yang, V. F. Fiore, T. H. Barker, Y. Sun, S. W. Morris, Q. Ding, V. J. Thannickal, Y. Zhou, *Am J Respir Cell Mol Biol* **2012**, 47, 340.
[35] A. J. Ford, P. Rajagopalan, *ACS Biomater Sci Eng* **2018**, 4, 3974.
[36] G. Thrivikraman, A. Jagiello, V. K. Lai, S. L. Johnson, M. Keating, A. Nelson, B. Schultz, C. M. Wang, A. J. Levine, E. L. Botvinick, R. T. Tranquillo, *Proc Natl Acad Sci U S A* **2021**, 118.
[37] a) B. Trappmann, B. M. Baker, W. J. Polacheck, C. K. Choi, J. A. Burdick, C. S. Chen, *Nat Commun* **2017**, 8, 371; b) H. Long, B. E. Vos, T. Betz, B. M. Baker, B. Trappmann, *Adv Sci (Weinh)* **2022**, 9, e2105325.
[38] a) J. Kastelic, A. Galeski, E. Baer, *Connect Tissue Res* **1978**, 6, 11; b) S. Thomopoulos, W. C. Parks, D. B. Rifkin, K. A. Derwin, *J Orthop Res* **2015**, 33, 832.
[39] a) K. Baghy, R. V. Iozzo, I. Kovalszky, *J Histochem Cytochem* **2012**, 60, 262; b) S. Bhattacharyya, K. S. Midwood, J. Varga, *Semin Cell Dev Biol* **2022**, 128, 130.
[40] L. Rittie, *Methods Mol Biol* **2017**, 1627, 395.
[41] D. Duscher, M. A. Schiffman, *Regenerative Medicine and Plastic Surgery: Skin and Soft Tissue, Bone, Cartilage, Muscle, Tendon, and Nerves*, Springer International Publishing, Charm, Switzerland **2019**.
[42] B. M. Baker, B. Trappmann, W. Y. Wang, M. S. Sakar, I. L. Kim, V. B. Shenoy, J. A. Burdick, C. S. Chen, *Nat Mater* **2015**, 14, 1262.

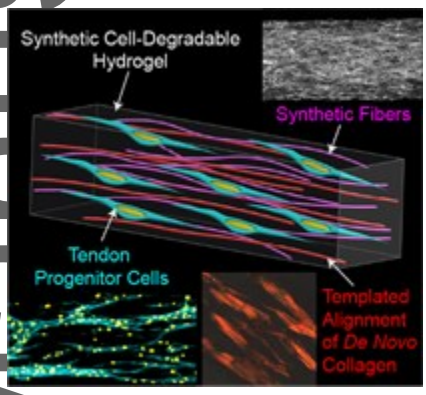
This article is protected by copyright. All rights reserved.

[43] a) A. M. Murthi, C. L. Vosburgh, T. J. Neviaser, *J Shoulder Elbow Surg* **2000**, 9, 382; b) A. C. van der Vlist, S. J. Breda, E. H. G. Oei, J. A. N. Verhaar, R. J. de Vos, *Br J Sports Med* **2019**, 53, 1352.

[44] a) A. D. Schoenenberger, J. Foolen, P. Moor, U. Silvan, J. G. Snedeker, *Acta Biomater* **2018**, 71, 306; b) E. Chung, Y. Son, *Tiss Eng Regen Med* **2014**, 11, 431; c) K. L. Spiller, S. Nassiri, C. E. Witherel, R. R. Anfang, J. Ng, K. R. Nakazawa, T. Yu, G. Vunjak-Novakovic, *Biomaterials* **2015**, 37, 194.

Author Manuscript

Table of Contents



Fiber-reinforced hydrogel composites were employed to elucidate salient microenvironmental determinants of tenogenesis and aligned collagen deposition by tendon progenitor cells. Culture in these soft, 3D microenvironments potentiated transforming growth factor β3-mediated tenogenic differentiation of tendon progenitor cells, and fibrous topographical anisotropy templated alignment of *de novo* collagen fibrils. These findings inform the design of cell-free, injectable hydrogels for tendon tissue regeneration.

This article is protected by copyright. All rights reserved.